

Quantum Deep Reinforcement Learning for Robot Navigation Tasks

Dirk Heimann^{1,*}, Hans Hohenfeld^{1,*}, Felix Wiebe^{2,*} and Frank Kirchner^{1,2}

Abstract—In this work, we utilize Quantum Deep Reinforcement Learning as method to learn navigation tasks for a simple, wheeled robot in three simulated environments of increasing complexity. We show similar performance of a parameterized quantum circuit trained with well established deep reinforcement learning techniques in a hybrid quantum-classical setup compared to a classical baseline. To our knowledge this is the first demonstration of quantum machine learning (QML) for robotic behaviors. Thus, we establish robotics as a viable field of study for QML algorithms and henceforth quantum computing and quantum machine learning as potential techniques for future advancements in autonomous robotics. Beyond that, we discuss current limitations of the presented approach as well as future research directions in the field of quantum machine learning for autonomous robots.

Index Terms—AI-Enabled Robotics, Autonomous Agents, Reinforcement Learning, Quantum Computing, Quantum Machine Learning

I. INTRODUCTION

Classical techniques for deep reinforcement learning for robotic behaviors have produced impressive results [1, 2, 3, 4], but they suffer from enormous sample complexity, limited generalization capabilities and limited applicability for flexible long-term autonomy ([5] provides an excellent overview of many of the challenges deep reinforcement learning is facing). Quantum computing promises the availability of computational resources far beyond the possibilities of classical computers [6]. Therefore, a promising field for applications of quantum computing is artificial intelligence and especially autonomous robotics [7].

The quantum advantage has been shown for a variety of algorithms like the Grover search algorithm [8] or Shor’s algorithm for factorizing integers [9]. Recently, quantum supremacy [10] was demonstrated with a task of sampling the output of pseudo-random quantum circuits on a 53 qubit superconducting quantum processor within 200 seconds, which would take about 10,000 years on a classical, state-of-the-art supercomputer.

Current and near-term devices, so called Noisy Intermediate-Scale Quantum Computers (NISQ) are limited

This work was funded by the German Federal Ministry of Research and Education (BMBF) and German Aerospace Center e.V. (DLR e.V.) under project number 50RA2033 (DFKI) and 50RA2032 (University of Bremen) and is part of the ongoing project QINROS (Quantum Computing and Quantum Machine Learning for Intelligent and Robotic Systems).

* Dirk Heimann, Hans Hohenfeld and Felix Wiebe are co-first authors and contributed to this work equally.

¹Dirk Heimann, Hans Hohenfeld and Frank Kirchner are with the Robotics Research Group, University of Bremen, Robert-Hooke-Straße 1, 28359 Bremen, Germany. {dirk.heimann, hans.hohenfeld, frank.kirchner}@uni-bremen.de

²Felix Wiebe and Frank Kirchner are with the German Research Center for Artificial Intelligence - Robotics Innovation Center (DFKI RIC), Robert-Hooke-Straße 1, 28359 Bremen, Germany. {felix.wiebe, frank.kirchner}@dfki.de

in the number of qubits, coherence times and fidelity of operation [11, 12] but nevertheless can already be utilized for a variety of problems. Recently, the availability of powerful quantum computing simulation software [13, 14, 15], cloud-based services for these devices [16, 17, 18, 19] and the integration of quantum computing techniques in popular machine learning software frameworks [20, 21] has led to an increased research interest in quantum machine learning. One promising approach is the hybrid training of parameterized quantum circuits (PQCs), optimizing a parameterized quantum algorithm as function approximator with classical optimization techniques in a hybrid quantum-classical setup [22, 23].

While these techniques are studied in a variety of machine learning domains, quantum deep reinforcement learning has only recently attracted interest of the machine learning and quantum computing research community alike. Existing works [24, 25, 26, 27] demonstrate the applicability of hybrid quantum-classical approaches for reinforcement learning tasks with performances similar to classical algorithms, while learning significantly more compact models. However, their scope is currently limited to applications and evaluations in relatively simple benchmark environments mostly from the OpenAI gym suite [28].

Our main contribution in this work is the first demonstration of the feasibility of quantum deep reinforcement learning for a simulated robotic task. We apply the Double Deep Q-Network algorithm [29] with a parameterized quantum circuit as approximator for the Q-function to three simulated navigation tasks for a wheeled robot. We show that it is possible to solve this navigation task with a quantum simulator by using a number of qubits, gates and circuit depth which are within the reach of near term quantum computers. In addition, we compare two different encoding techniques and various circuit depths within each technique. Furthermore, we discuss various challenges and limitations of the presented method and potential areas of research for quantum machine learning to contribute to future advancements in autonomous robotics.

The rest of this paper is outlined as follows: In Section II we provide a brief overview on previous works regarding deep reinforcement learning with PQCs. Subsequently, we delineate the quantum deep reinforcement learning framework underlying this work in Section III. Afterwards, the learning setup with regards to the simulated environments and learning methods is documented in Section IV. We present the training results of the suggested methods compared to a classical baseline in Section V before summarizing our main findings, discussing their implications, limitations as well as potential future research directions in the concluding Section VI.

II. RELATED WORK

Quantum Deep Reinforcement Learning with parameterized quantum circuits is a relatively new field of research, therefore not many related previous works on this topic exist. Chen et al. [24] demonstrated an approach based on deep Q-networks for two benchmark environments with discrete state and action spaces using basis encoding [30] followed by CNOT entanglements and parameterized Pauli rotations. Lockwood et al. [25] worked with a similar circuit layout but introduced a different encoding technique and also combined the parameterized circuit with quantum pooling operations [31] and classical neural network layers showing similar performance to a classical DQN agent on a Cartpole and Black Jack environment. The two most recent works from Skolik et al. [27] and Jerbi et al. [26] use a circuit layout and encoding scheme similar to the one we employ in this work to train agents in various OpenAI Gym [28] environments with the Deep Q-network and REINFORCE algorithms respectively. In Jerbi et al. the authors additionally demonstrate experimentally and formally, that quantum deep reinforcement learning can solve several environments based on the discrete logarithm problem [32], which are intractable for classical learning methods.

The results from these works demonstrate the applicability of deep reinforcement learning with PQCs and hybrid quantum training of autonomous agents. While they compare different network structures and algorithms, their scope is limited to relatively simple benchmarking environments.

In contrast to those works, we extend the scope to a more realistic robotic scenario with a continuous state space and real-time simulated physics, thereby significantly expanding scope and complexity of scenarios for quantum deep reinforcement learning.

III. QUANTUM DEEP REINFORCEMENT LEARNING

A. Double Deep Q-Networks

For all our experiments, we used the Double Deep Q-Network (DDQN) [29] algorithm as it performed slightly better on average as e. g., the basic Deep Q-Network algorithm (DQN) [33]. The DDQN is a model-free, off-policy deep reinforcement learning algorithm that uses a neural network to approximate the Q-function from the basic Q-learning algorithm [34]. In reinforcement learning scenarios an agent is trained to maximize a scalar reward by acting within an environment. The agent learns solely from its interactions with the environment without any direct instructions. At each time step $t \in \mathbb{N}$ the agent observes a state s_t from the set of possible states S . For the DDQN algorithm, the agent then picks an action a_t from its discrete action set A following an ϵ -greedy policy. That is, with probability $\epsilon \in [0, 1]$ the agent performs a random action $a_t \in A$ and with probability $1 - \epsilon$ the best action according to the current estimation of the Q-function:

$$a_t = \operatorname{argmax}_a Q_\theta(s_t, a). \quad (1)$$

$Q_\theta(s, a)$ is a function assigning a value to each state and action combination and is approximated by a neural

network with parameters θ . After performing a_t in the environment, the agent observes a new state s_{t+1} and receives a scalar reward $r_{t+1} = r(s_t, a_t, s_{t+1})$. The interaction $(s_t, a_t, r_{t+1}, s_{t+1})$ is stored in a replay buffer [35] from which at a predefined interval, e. g. at each time step, a mini-batch of interactions is sampled to update Q_θ with stochastic gradient descent, minimizing the loss $(y_t - Q_\theta(s_t, a_t))^2$, with y_t given by

$$y_t = r_{t+1} + \gamma Q_{\theta'}(s_{t+1}, \operatorname{argmax}_{a'} Q_\theta(s_{t+1}, a')). \quad (2)$$

$Q_{\theta'}$ is a target network of identical structure as Q_θ that gets updated periodically with $\theta' = \theta$ and is used to stabilize the training process [33]. $\gamma \in (0, 1)$ is a discount factor controlling the preference of short term over long term rewards. For a more in-depth treatment of the DDQN algorithm we refer to [29].

B. Quantum Computing

We give a short introduction into common notation of quantum computing and refer the interested reader to [36] for a comprehensive explanation of basic and advanced concepts of this topic. The fundamental objects in quantum computing are qubits, which are the analogon to bits in classical computing. Unlike classical bits, which can be in one of the two states 0 and 1, a qubit can be in a state, which is a linear combination of those states. Using the bra-ket notation, a qubit state $|\Psi\rangle$ can be written as

$$|\Psi\rangle = \alpha |0\rangle + \beta |1\rangle, \text{ with } \alpha, \beta \in \mathbb{C}, |\alpha|^2 + |\beta|^2 = 1, \quad (3)$$

where $|0\rangle$ and $|1\rangle$ are basis states of the underlying single-qubit Hilbert Space. During the probabilistic measurement process, the qubit will collapse to one of the two basis states and $|\alpha|^2$ and $|\beta|^2$ can be interpreted as the probabilities for the respective basis states. Before the measurement, the state can be modified by applying quantum gates U

$$|\Psi'\rangle = U |\Psi\rangle \quad (4)$$

which are formally described by unitary operators U .

This formulation can be extended to multi-qubit systems by preparing an n -qubit quantum register. For quantum computers, this is commonly initialized in its computational basis state $|0\rangle^{\otimes n}$.

C. Parameterized Quantum Circuits for Deep Reinforcement Learning

Variational quantum algorithms are a promising method to implement algorithms on current and near-term quantum computers as they are well suited for systems with a relative small number of qubits, noisy operation and limited coherence times [37]. Their basic principle of operation is the combination of a parameterized quantum circuit whose parameters are adjusted by a classical optimizer towards the desired outcome while evaluating the quantum circuit with adjusted parameters at each optimization step [38]. First introduced in the context

of variational quantum eigensolvers [39], they became a major research area in quantum machine learning [38, 40, 41, 42].

A parameterized quantum circuit (PQC) is a series of quantum gates $U(\boldsymbol{\theta}, \mathbf{x})$ which is applied to the computational basis of n qubits $|0\rangle^{\otimes n}$. These gates are parameterized by variational parameters $\boldsymbol{\theta}$ and classical input data \mathbf{x} . Fig. 1 depicts this general ansatz for a machine learning application.

The PQC's quantum state $|U(\boldsymbol{\theta}, \mathbf{x})\rangle = U(\boldsymbol{\theta}, \mathbf{x})|0\rangle^{\otimes n}$ is computed and measured for many repeated iterations to gather sufficient statistics for the expectation value

$$\langle \mathcal{O} \rangle = \langle U(\mathbf{x}, \boldsymbol{\theta}) | \mathcal{O} | U(\boldsymbol{\theta}, \mathbf{x}) \rangle \quad (5)$$

for an observable \mathcal{O} . $\langle U(\mathbf{x}, \boldsymbol{\theta}) |$ denotes the conjugate transpose of $|U(\boldsymbol{\theta}, \mathbf{x})\rangle$.

The measured expectation value of the quantum computation can be interpreted as the computation of a parameterized function $f_{\mathcal{O}}(\boldsymbol{\theta}, \mathbf{x})$ depending on the observable, circuit parameters and input.

The parameters $\boldsymbol{\theta}$ are tuned with an appropriate method to fit a target function. E.g. in the domain of supervised machine learning a loss function \mathcal{L} can be minimized by performing gradient descent in $\nabla_{\boldsymbol{\theta}} \mathcal{L}$. Several analytic and numeric methods allow for calculating gradients of quantum circuits with respect to their parameters [43, 44, 45].

A critical aspect is how classical data can be encoded into a PQC. Various encoding methods for quantum machine learning tasks have been suggested [30] but recent results on the expressiveness of quantum circuits emphasize the advantages of repeated encodings, also referred to as data re-upload [41, 46]. Such an ansatz enables the circuit to compute functions of the form

$$f(\boldsymbol{\theta}, \mathbf{x}) = \sum_{\omega \in \Omega} c_{\omega}(\boldsymbol{\theta}) e^{i\omega \mathbf{x}}, \quad (6)$$

which is a partial Fourier series with frequency spectrum Ω depending on data encoding, and coefficients $c_{\omega}(\boldsymbol{\theta})$ determined by trained variational parameters $\boldsymbol{\theta}$ [41].

PQCs with data re-upload have L layers which consist of data encoding unitaries $U_{\text{in}}(\mathbf{x}_l)$ followed by parameterized unitaries $\tilde{U}(\boldsymbol{\theta}_l)$ in each layer l . As introduced in [41], the circuit starts with parameterized unitaries $\tilde{U}(\boldsymbol{\theta}_0)$ applied on the n -qubit register $|0\rangle^{\otimes n}$ followed by a sequential implementation of the layers. Fig. 2 depicts the circuit layout for such an ansatz.

In the following, we explain in detail how to construct PQCs for real valued input data. This enables quantum

$$|0\rangle^{\otimes n} \xrightarrow{U(\boldsymbol{\theta}, \mathbf{x})} \langle \mathcal{O} \rangle =: f_{\mathcal{O}}(\boldsymbol{\theta}, \mathbf{x})$$

Fig. 1: Basic principle of a parameterized quantum circuit (PQC). An arbitrary unitary $U(\boldsymbol{\theta}, \mathbf{x})$, which may be composed of any number of quantum gates, is applied to an n qubit register initialized in its basis state. The unitary is parameterized by parameters $\boldsymbol{\theta}$ and input \mathbf{x} . Thereby, the expectation value of an observable $\langle \mathcal{O} \rangle$ can be defined as a parameterized function $f_{\mathcal{O}}(\boldsymbol{\theta}, \mathbf{x})$.

enhanced deep Q-learning for robotics, with continuous states $\mathbf{s} \in S$ with n_s state features.

We consider two different re-upload strategies resulting in two different implementations of $U_{\text{in}}(\mathbf{x}_l)$. In the first case, we follow [27] by rescaling each continuous classical feature s_i of the state \mathbf{s} with trainable parameters ξ_{li} for each layer l using the function $x_{li} = \arctan(\xi_{li}s_i) \in [-\pi, \pi]$. The index sets of the trainable input parameters are given by $i \in \{1, \dots, n_s\}$ and $l \in \{1, \dots, L\}$ resulting in Ln_s parameters. In the following, \mathbf{x} denotes the set of all encoded and rescaled input data and \mathbf{x}_l a subset of all encoded and rescaled input data for layer l . In this encoding style each state feature s_i is encoded on one qubit:

$$\mathbf{s} \mapsto U_{\text{in},1}(\mathbf{x}_l(\mathbf{s})) = \bigotimes_{q=1}^n U_{\text{in},1}^{(q)}(x_{lq}), \quad (7)$$

where $U_{\text{in},1}^{(q)}$ is one of the Pauli rotations R_x, R_y, R_z with rotation angle x_{lq} depending on state feature s_q acting on qubit q . For this type of encoding the number of qubits n has to be equal to the number of input features n_s .

In the second case we encode, in line with [46], three features of the rescaled state \mathbf{s} in a universal, single qubit gate $U_{\text{in},3}^{(q)}$ composed of three parameterized Pauli rotation gates. Any combination of rotation gates capable of representing a general three dimensional rotation, e.g. $R_x R_y R_x$, suffices for $U_{\text{in},3}^{(q)}$. The state features s_i are encoded as the rotation angles. Therefore, the rescaling is done by using different trainable variables ξ_{li}^q for each qubit $q \in \{1, \dots, n\}$, which formally can be written as: $x_{li}^q = \arctan(\xi_{li}^q s_i) \in [-\pi, \pi]$. This encoding uses nLn_s trainable input parameters. Similar to the first encoding, all trainable parameters used for layer l are denoted by \mathbf{x}_l . A state \mathbf{s} is encoded as:

$$\mathbf{s} \mapsto U_{\text{in},3}(\mathbf{x}_l(\mathbf{s})) = \bigotimes_{q=1}^n U_{\text{in},3}^{(q)}(x_{l1}^q, x_{l2}^q, x_{l3}^q). \quad (8)$$

For a state space with more than three features, $U_{\text{in},3}$ would be repeated until all features are encoded. Each $U_{\text{in},3}$ then encodes a subset of three features, potentially padding the state space with features set to 0 to make its dimensionality divisible by 3 [46]. We perform experiments with both encoding styles, $U_{\text{in},1}(\mathbf{x})$ and $U_{\text{in},3}(\mathbf{x})$, and unify the notation by referring to both with $U_{\text{in}}(\mathbf{x})$.

The parameterized part of the PQC, $\tilde{U}(\boldsymbol{\theta})$, consists of two

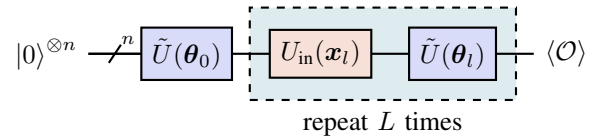


Fig. 2: Data re-upload in parameterized quantum circuits: After an initial parameterized unitary $\tilde{U}(\boldsymbol{\theta}_0)$, L layers of data encoding unitaries $U_{\text{in}}(\mathbf{x}_l)$ and parameterized unitaries $\tilde{U}(\boldsymbol{\theta}_l)$ are applied to the n qubit quantum register.

parts. One part includes universal, single-qubit gates:

$$U_{\text{par}}(\boldsymbol{\theta}_l) = \bigotimes_{q=1}^n U_{\text{par}}^{(q)}(\theta_{l1}^q, \theta_{l2}^q, \theta_{l3}^q), \quad (9)$$

which can be implemented by any general, parameterized rotation with three Pauli-rotation gates contributing $3nL$ trainable circuit parameters. The second part contains fixed entangling gates U_{ent} to create entanglement by acting on all n qubits. We choose controlled Z gates on all neighboring pairs of qubits and between the last and the first qubit.

Combining all segments, the PQC ansatz with data reupload is constructed by applying the parameterized part $\tilde{U}(\boldsymbol{\theta}_0)$ to the initial register followed by a layer of data encoding $U_{\text{in}}(\mathbf{x}_l)$ and another parameterized part $\tilde{U}(\boldsymbol{\theta}_l)$ which are repeated L times. The entire circuit is given by:

$$U(\boldsymbol{\theta}, \mathbf{x}) = \prod_{l=1}^L \left(U_{\text{ent}} U_{\text{par}}(\boldsymbol{\theta}_l) U_{\text{in}}(\mathbf{x}_l) \right) U_{\text{ent}} U_{\text{par}}(\boldsymbol{\theta}_0). \quad (10)$$

This operator is applied to the initial state $|0\rangle^{\otimes n}$ leading to the final state $|U(\boldsymbol{\theta}, \mathbf{x})\rangle$. and the expectation value of an observable \mathcal{O} :

$$\begin{aligned} f_{\mathcal{O}}(\boldsymbol{\theta}, \mathbf{s}) &:= \langle \mathcal{O} \rangle_{\boldsymbol{\theta}, \mathbf{s}} \\ &= \langle U(\mathbf{x}(\mathbf{s}), \boldsymbol{\theta}) | \mathcal{O} | U(\boldsymbol{\theta}, \mathbf{x}(\mathbf{s})) \rangle. \end{aligned} \quad (11)$$

As observables, we choose Pauli-z gates $\{\sigma_z^{(1)}, \dots, \sigma_z^{(n)}\}$ each acting on another qubit to obtain n different output values. The output values can either be directly interpreted as values for $Q(\mathbf{s}, a)$ in the reinforcement learning scenario or combined, scaled or further post-processed by any classical means including additional classical neural network layers.

Let a_j be one action of the action space $A = \{a_0, \dots, a_{n_a}\}$ with $n_a \leq n_s$. If $n_a < n_s$, the PQC output values could be combined, e.g. by multiplying some of them [27], to reduce the number of output values to the number of possible actions n_a . For simplicity, we assume that $n_a = n_s$ which means that the PQC output value $\langle \sigma_z^{(i)} \rangle_{\boldsymbol{\theta}, \mathbf{s}} \in [-1, 1]$ can directly correspond to the Q-value of action a_i .

In our learning scenario, the Q-values range exceeds the interval $[-1, 1]$ and therefore need additional post-processing. The authors of [27] suggest rescaling each output value with an additional trainable parameter w_j :

$$Q(\mathbf{s}, a_j) = \langle \sigma_z^{(j)} \rangle_{\boldsymbol{\theta}, \mathbf{s}} \cdot w_j, \quad (12)$$

which adds n_a trainable output variables to the model.

IV. LEARNING SETUP

A. Environment

In our experiments, we use three environments based on a simulated Turtlebot2 robot¹. We chose this robotic system as it allows for relatively simple, yet realistic navigation tasks while being a readily available and extensible system which we can build upon in future work. It is controlled via two

independent motors by setting target velocities for its two wheels.

The environments are depicted in Fig. 3: The 3x3 environment shown in Fig. 3a as smallest, the 4x4 environment (Fig. 3b) of medium size and the largest 5x5 environment (Fig. 3c). In each environment, the robot starts at a fixed position in the upper left corner and has to navigate to a fixed goal position marked with a green sphere while avoiding collisions with the outer walls and the obstacles within the environment. We created all environments with the pybullet [47] real-time physics engine and set a control frequency of 100Hz for collision detection and calculating forward dynamics.

The robot has three actions available (forward, turn left, turn right) to move in the environments. To move forward, the same target velocity is applied to both wheels, whereas for turning left and right, equal velocities but with opposing directions are set. An action is chosen every 50 simulation steps, corresponding to an execution time of 0.5 seconds. With this control scheme, the robot needs about 20 consecutive actions to reach the goal in the 3x3 environment on a near optimal trajectory, 30 steps in the 4x4 environment and 45 steps in the large 5x5 environment respectively.

All three environments have the same state space with three components. The first two are the robot's position in the plain in x and y coordinates, the third is its orientation around the z axis in radians.

We use the same simple, yet informative reward function to train the robot in all environments. For reaching the goal, a reward of 10.0 is granted, a collision is penalized with -1.0. For all other steps, the agent receives 0.1 upon decreasing the distance to the goal and -0.2 else. The penalty term ensures shorter trajectories are preferred by the agent. We consider the environments solved when a total reward of 10.5 (3x3), 11.0 (4x4) and 10.0 (5x5) is reached. We allow for some tolerance on the length of the trajectory and the exact route, therefore these thresholds are a lower bound based on several manually determined valid trajectories, making slightly larger total rewards possible.

In all environments an episode ends, when the robot reaches the goal, collides with an object or a maximum number of 200 steps was executed during training.

B. Learning

We trained the simulated robot using three different paradigms: A baseline with classical neural networks for both Q-functions and two different parameterized quantum circuits as function approximators.

For the classical baseline agent, we employ a simple, three layer, fully connected neural network with rectified linear unit activation on all but the final layer, which has a linear activation. We performed training runs with different numbers of units in both hidden layers (see Section V) and a learning rate of 0.001.

In both quantum cases, we build our circuit on a total of three qubits, which aligns well with the dimensionality of our state space and the number of actions available to the agent. Both circuits follow the general approach depicted in Fig. 2

¹<https://www.turtlebot.com/turtlebot2/>

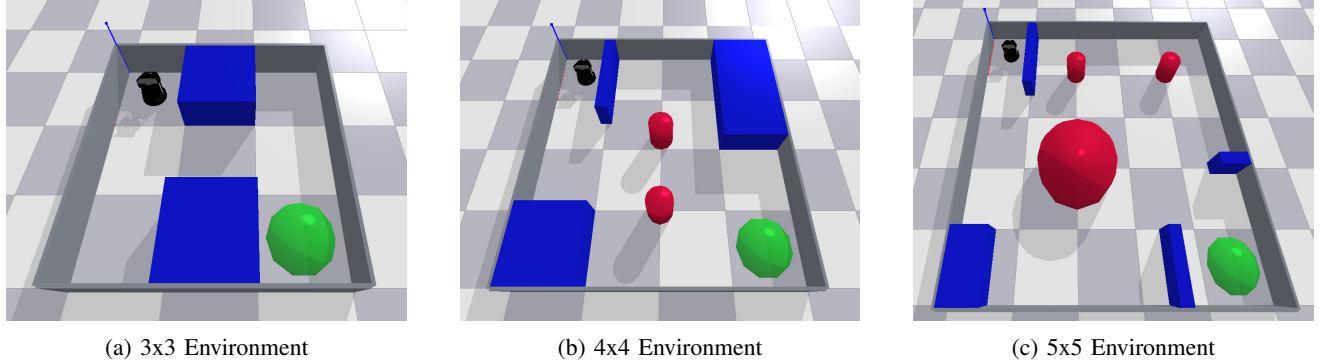


Fig. 3: The three different simulated navigation environment for the Turtlebot 2 robot. In each, the robot has to navigate from its starting position in the upper left corner to the position marked with a green circle in the lower right while avoiding collisions with the enclosing walls and any obstacles. With the configured control scheme, this takes about 20 steps in the 3x3 environment (3a), 30 in the 4x4 (3b) and 45 steps in the 5x5 environment (3c) for a (near) optimal trajectory.

and are only different in their data encoding structure U_{in} and the number of layers L used. The circuit layout for a single layer l is illustrated in Fig. 4.

Our first data re-upload PQC model uses the encoding $U_{\text{in},1}^{(q)}$ on each qubit with the rotation gate R_x to encode one state feature on one qubit each (PQC-1). For the second model we use $U_{\text{in},3}^{(q)}$ for each qubit with rotation gates $R_x R_y R_x$ to encode every state feature on one qubit (PQC-3). The universal rotation $U_{\text{par}}^{(q)}$ on each qubit is composed of three parameterized Pauli rotation gates $R_x R_y R_z$.

The training with both quantum models was performed with several different settings for the depth of the circuit in all three environments. We used the same learning rates of 0.001 for the variational parameters and 0.01 for the input and output scaling during all experiments.

The replay buffer for the learning algorithm was set to a capacity of 20,000 experience samples. For each training step, a mini-batch of 64 samples is drawn from the buffer. Exploration is handled with an ϵ -greedy policy, starting at $\epsilon = 1.0$ and gradually reducing it to 0.1 towards the end of each training run. Training time is limited to 50,000 training steps for all environments. The learned policy is evaluated in 10 consecutive runs after every 100 training steps. Once an average evaluation reward greater than the success criterion for the environment is reached, training is stopped early.

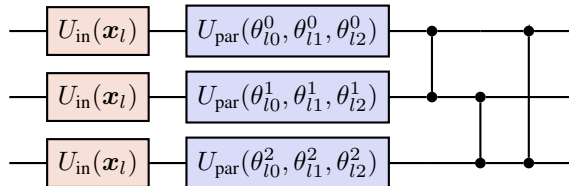


Fig. 4: Circuit layout for layer l of our PQC ansatz. The encoding unitary U_{in} on each qubit q is given by $U_{\text{in},1}^{(q)}$, resp. $U_{\text{in},3}^{(q)}$. It is followed by a general rotation gate U_{par} with three variational parameters $\theta_{10}^q, \theta_{11}^q, \theta_{12}^q$ for each qubit and a full entanglement among all qubits with three controlled-Z gates. We omit the qubit index on all gates for readability.

All hyper-parameters were determined empirically and tuned for optimal performance, stability during training and reproducibility of results across multiple runs.

V. RESULTS

Using the hyper-parameters outlined in the previous section, we trained the robot with models of different sizes in all three environments. For the classical baseline (DDQN), we employed seven different neural networks with increasing number of units for both hidden layers. The parameterized quantum circuits with one rotation gate as encoding unitary (PQC-1) as well as with three gates per encoding (PQC-3) were trained with five different circuit depths for each input configuration. For each paradigm and environment, we started our training runs with one of the smaller configurations. An increase or decrease of model size was only considered for subsequent runs, until no further significant improvement or a decrease in performance was observed.

For a total of 43 different configurations, we performed 20 consecutive training runs for each. In Table I, all used models and the number of hidden units or circuit layers L are summarized. Furthermore, the number of successful training runs (succ.) as well as the mean training duration for the best 10 runs (\bar{t}) are shown.

During the experiments, several trends emerged. With all three training paradigms, we were able to solve all environments successfully, but in terms of training time the classical baseline usually performed better. This is especially true for the smallest environment, but becomes less clear with increasing size and complexity of the task. Comparing both types of quantum circuits, the PQC-3 models outperformed the PQC-1 models consistently in terms of training speed and show comparable performance to the classical baseline in that regard. At least for the tasks considered in this work, more input encodings and trainable scaling parameters for the encoding seem more favorable than more variational parameters and entangling gates. These findings are further emphasized by the learning curves depicted in Figure 5. The top row shows the learning progress for the classical baseline in each environment, whereas the quantum models

TABLE I: Models used for all experiments grouped by classical baseline (DDQN), and the two parameterized quantum circuits (PQC-1 and PQC-3). For each model the table shows the number of hidden units or Layers L and trainable parameters $|\theta|$. For each environment the number of successful training runs (*suc.*) and the average amount of training steps for the best 10 runs (\bar{t}) is outlined.

	Model		3x3 env.		4x4 env.		5x5 env.	
	units	$ \theta $	suc.	\bar{t}	suc.	\bar{t}	suc.	\bar{t}
DDQN	8;8	131	17	22,630	16	29,750	—	—
	16;8	227	20	17,470	17	30,050	—	—
	16;16	387	20	13,960	17	14,730	8	43,140
	32;16	707	20	12,350	17	19,760	15	36,490
	32;32	1238	20	10,860	16	14,920	17	32,780
	64;32	2435	20	8,680	20	10,710	18	26,380
	64;64	4611	17	8,670	20	11,430	20	26,390
PQC-1	Model		3x3 env.		4x4 env.		5x5 env.	
	L	$ \theta $	suc.	\bar{t}	suc.	\bar{t}	suc.	\bar{t}
	12	156	20	21,700	18	37,040	—	—
	15	192	20	16,070	20	23,010	12	43,130
	18	228	20	17,450	20	18,340	18	35,500
	21	264	—	—	20	19,250	20	31,800
24	300	—	—	—	—	20	31,040	
PQC-3	Model		3x3 env.		4x4 env.		5x5 env.	
	L	$ \theta $	suc.	\bar{t}	suc.	\bar{t}	suc.	\bar{t}
	8	156	20	17,260	20	22,770	13	38,640
	10	192	20	10,890	20	19,020	18	35,830
	12	228	20	13,340	20	15,700	20	30,240
	14	264	—	—	20	13,780	20	29,420
16	300	—	—	20	16,250	20	28,070	

are compared in the bottom rows. Each plot shows the mean evaluation reward of the best 10 out of 20 runs for each tested configuration. Comparing the classical baseline with the quantum models, the shorter training times become apparent, as well as the overall better performance of the PQC-3 models when compared to PQC-1 models with equal number of parameters. Similar to the findings from the mean duration alone, the differences become less clear, albeit still visible, for the more challenging environments.

Another noteworthy result, which is in line with previous findings from the quantum deep reinforcement learning research, is the fact that both quantum models were capable of solving the environments with one order of magnitude less trainable parameters, when considering the best performing models. The overall best classical baseline model with 64 and 32 hidden units has 2434 parameters, whereas the best performing quantum models only employ between 192 and 300 trainable parameters. We still were able to solve the two smaller environments with comparably small classical models but at the expense of significantly increased training times.

VI. DISCUSSION

In this work, we investigated and demonstrated the potential for quantum deep reinforcement learning as a method to learn autonomous robotic behaviors. The hybrid quantum-classical algorithmic setup shows comparable performance with the classical deep reinforcement learning baseline, while

learning behaviors in more compact models. For the smallest environment, the classical baseline models only outperformed the quantum models in terms of training duration, whereas this effect became less significant with increasing complexity of the task. From these results multiple future research prospects arise.

First, from a perspective of quantum machine learning in general and quantum deep reinforcement learning specifically, more research regarding the scaling behavior of current state of the art methods based on hybrid optimization of PQCs is needed. This includes the comparison to classical machine learning as well as analyzing the impact of barren plateaus [48]. In our experiments, smaller tasks and henceforth smaller quantum circuits seem less favorable for the PQC approach, although this is only indicated by a small number of experiments and limited setting. Additional research with more and more demanding tasks is needed to produce more conclusive results.

The second area we see as equally important, is the applicability of quantum machine learning and quantum deep reinforcement learning in real-world applications, especially in the field of robotics. While we have demonstrated quantum deep reinforcement learning in a limited robotic scenario, actual advantages of the presented method over classical deep reinforcement learning have yet to be shown. While previous works demonstrated a quantum advantage for a certain class of problems [26] intractable for classical learning methods, it is unclear how this translates to problems from e. g., robotic domains.

Another crucial topic is the encoding scheme of classical data into the quantum circuit. With the proposed methods, the required number of qubits and/or the operations per qubit, i.e. the coherence time, scales in the best case linearly with the dimensionality of the state space. As shown by [41] for the case of the data-reupload encoding, the data encoding style directly influences the type of functions which the quantum circuit is able to express. It will be interesting to see how different encoding techniques like e. g., amplitude encoding [49] would impact the learning behavior.

Furthermore, we limited our experiments to state spaces of very small dimensionality to account for the limitations of current NISQ devices and the computational demands for simulation quantum circuits on a classical computer. While this imposed no detriments on our learning scenarios, having very high dimensional sensory data is not uncommon in more complex robotic tasks. How to encode classical data with hundreds, thousands or more dimensions efficiently onto quantum devices with their current limitations is an open question. Investigating classical pre-processing, compression and dimensionality reduction techniques in this context could potentially enable quantum deep reinforcement learning for such scenarios.

Additionally, the scope of our work is limited with regards to actual quantum hardware and its properties. We performed all our experiments with a quantum simulator which enabled us to employ circuits with a depth beyond what current hardware is able to support and also removed the necessity to deal with the noise that typically comes with the execution

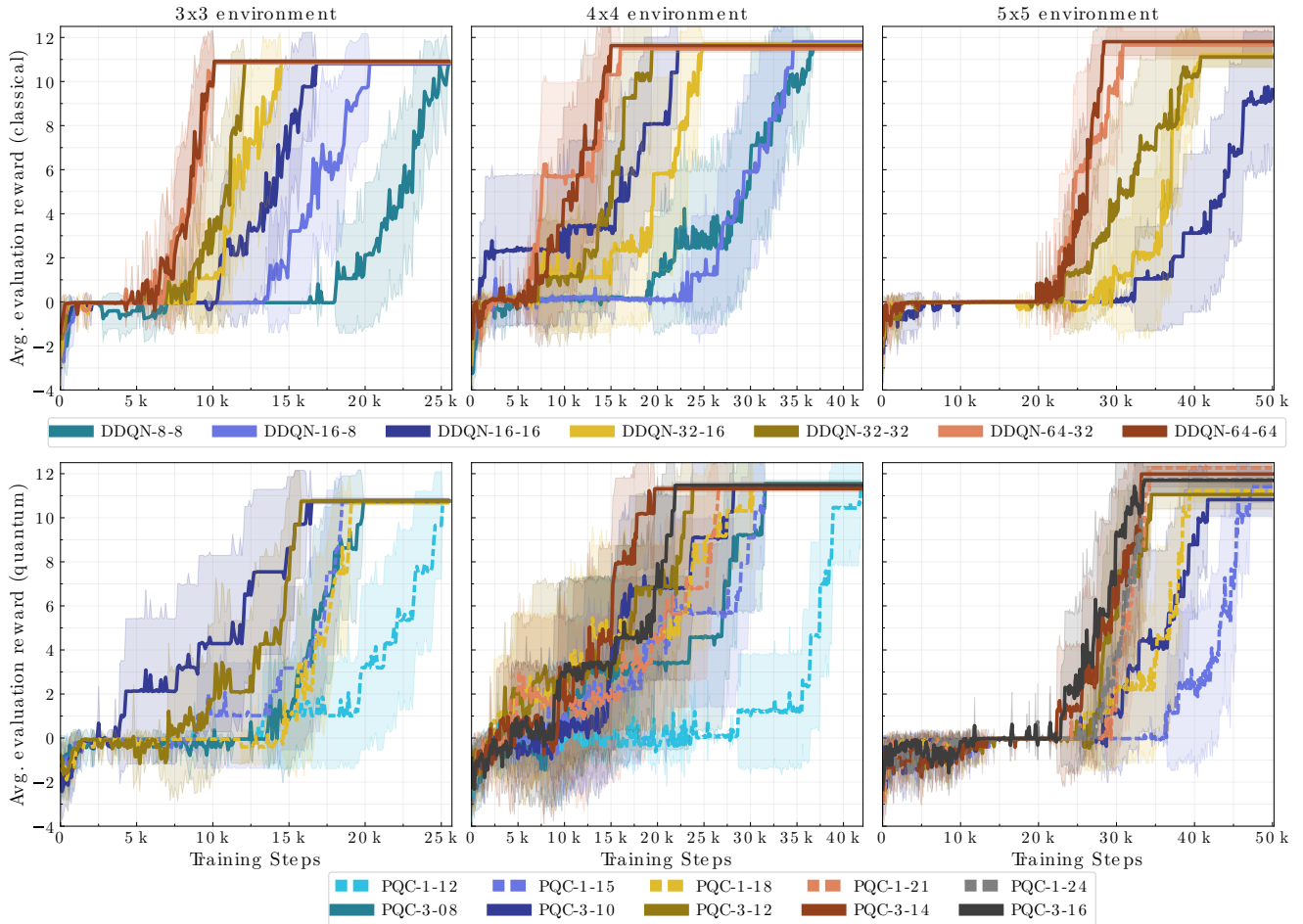


Fig. 5: Evaluation results of all three environments for the best 10 out of 20 runs. Each plot shows the mean evaluation performance over 10 consecutive runs with the trained policy, whereby negative rewards are rescaled by a factor of 0.1 to improve readability. The evaluation was performed every 100 training steps and training stopped, once the environment was solved with the policy. Plots are padded with additional evaluation runs to have equal lengths for better comparability. The outline of each plot is the 95% confidence interval.

of algorithms on current quantum hardware. The execution of even simpler machine learning tasks on actual quantum hardware would be further limited by their sparse availability, complexity and high usage cost. To circumvent these issues, research into techniques to combine quantum simulators and quantum hardware in an efficient training setup could be a practical route forward.

Lastly, we understand our work as a contribution towards application focused, empirical research on quantum algorithms in a robotic context. On one hand, we see this as a viable route forward to accelerate the development and understanding of quantum algorithms, quantum machine learning and specifically the application of quantum techniques in deep reinforcement learning. On the other hand, we strongly believe that these types of algorithms together with future hardware developments in the field of quantum computing will greatly contribute to the advancement of autonomous robotics.

VII. ACKNOWLEDGMENTS

We thank Patrick Draheim, Melvin Laux and Alexander Fabisch for their valuable feedback on this manuscript.

REFERENCES

- [1] M. Andrychowicz *et al.*, “Learning Dexterous In-Hand Manipulation,” *The International Journal of Robotics Research*, vol. 39, no. 1, pp. 3–20, 2020.
- [2] D. Kalashnikov *et al.*, “Scalable Deep Reinforcement Learning for Vision-Based Robotic Manipulation,” in *Proceedings of The 2nd Conference on Robot Learning*, ser. Proceedings of Machine Learning Research, A. Billard, A. Dragan, J. Peters, and J. Morimoto, Eds., vol. 87. PMLR, 29–31 Oct 2018, pp. 651–673.
- [3] A. R. Mahmood, D. Korenkevych, G. Vasan, W. Ma, and J. Bergstra, “Benchmarking Reinforcement Learning Algorithms on Real-World Robots,” in *Proceedings of The 2nd Conference on Robot Learning*. PMLR, Oct. 2018, pp. 561–591.
- [4] S. Gu, E. Holly, T. Lillicrap, and S. Levine, “Deep Reinforcement Learning for Robotic Manipulation with Asynchronous Off-Policy Updates,” in *2017 IEEE International Conference on Robotics and Automation (ICRA)*, 2017, pp. 3389–3396.
- [5] A. Irpan, “Deep Reinforcement Learning Doesn’t Work Yet,” 2018. [Online]. Available: <https://www.alexirpan.com/2018/02/14/rl-hard.html>
- [6] A. Montanaro, “Quantum algorithms: an overview,” *npj Quantum Information*, vol. 2, no. 1, 2016.
- [7] F. Kirchner, “AI-Perspectives: The Turing Option,” *AI Perspectives*, vol. 2, no. 1, pp. 1–12, 2020.
- [8] L. K. Grover, “A Fast Quantum Mechanical Algorithm for Database Search,” in *Proceedings of the Twenty-Eighth Annual ACM Symposium*

- on *Theory of Computing*. New York, NY, USA: Association for Computing Machinery, 1996, p. 212–219.
- [9] P. Shor, “Algorithms for Quantum Computation: Discrete Logarithms and Factoring,” in *Proceedings 35th Annual Symposium on Foundations of Computer Science*, 1994, pp. 124–134.
- [10] F. Arute *et al.*, “Quantum Supremacy Using a Programmable Superconducting Processor,” *Nature*, vol. 574, no. 7779, pp. 505–510, 2019.
- [11] J. Preskill, “Quantum Computing in the NISQ era and beyond,” *Quantum*, vol. 2, p. 79, 2018. [Online]. Available: <http://dx.doi.org/10.22331/q-2018-08-06-79>
- [12] M. Brooks, “Beyond Quantum Supremacy: The Hunt for Useful Quantum Computers,” *Nature*, vol. 574, no. 7776, pp. 19–21, 2019.
- [13] Quantum AI team and collaborators, *Qsim*, 2020. [Online]. Available: <https://doi.org/10.5281/zenodo.4023103>
- [14] B. Villalonga *et al.*, “A Flexible High-Performance Simulator for Verifying and Benchmarking Quantum Circuits Implemented on Real Hardware,” *npj Quantum Inf*, vol. 5, no. 1, pp. 1–16, 2019.
- [15] J. Gray, “Quimb: A Python Package for Quantum Information and Many-Body Calculations,” *Journal of Open Source Software*, vol. 3, no. 29, p. 819, Sep. 2018.
- [16] IBM, *IBM Quantum Experience*, IBM Quantum. [Online]. Available: <https://quantum-computing.ibm.com/>
- [17] Google, *Quantum Computing Service — Google Quantum AI*, 2021. [Online]. Available: <https://quantumai.google/quantum-computing-service?hl=de>
- [18] Amazon, *Amazon Braket*, Amazon Web Services, Inc., 2021. [Online]. Available: <https://aws.amazon.com/braket/>
- [19] Rigetti, *Rigetti - Quantum Computing*, Rigetti Computing, 2021. [Online]. Available: <https://www.rigetti.com/>
- [20] M. Broughton *et al.*, “TensorFlow Quantum: A Software Framework for Quantum Machine Learning,” 2021, arXiv preprint arXiv:2003.02989. [Online]. Available: <http://arxiv.org/abs/2003.02989>
- [21] V. Bergholm *et al.*, “PennyLane: Automatic Differentiation of Hybrid Quantum-Classical Computations,” 2020, arXiv preprint arXiv:1811.04968. [Online]. Available: <http://arxiv.org/abs/1811.04968>
- [22] E. Farhi and H. Neven, “Classification with Quantum Neural Networks on Near Term Processors,” 2018, arXiv preprint arXiv:1802.06002. [Online]. Available: <https://arxiv.org/abs/1802.06002>
- [23] M. Benedetti, E. Lloyd, S. Sack, and M. Fiorentini, “Parameterized Quantum Circuits as Machine Learning Models,” *Quantum Science and Technology*, vol. 4, no. 4, p. 043001, 2019.
- [24] S. Y.-C. Chen, C.-H. H. Yang, J. Qi, P.-Y. Chen, X. Ma, and H.-S. Goan, “Variational Quantum Circuits for Deep Reinforcement Learning,” *IEEE Access*, vol. 8, pp. 141 007–141 024, 2020.
- [25] O. Lockwood and M. Si, “Reinforcement Learning with Quantum Variational Circuit,” in *AAAI Conference on Artificial Intelligence and Interactive Digital Entertainment*, vol. 16, no. 1, 2020, pp. 245–251.
- [26] S. Jerbi, C. Gyurik, S. Marshall, H. Briegel, and V. Dunjko, “Parametrized Quantum Policies for Reinforcement Learning,” in *Advances in Neural Information Processing Systems*, vol. 34, 2021.
- [27] A. Skolik, S. Jerbi, and V. Dunjko, “Quantum Agents in the Gym: A Variational Quantum Algorithm for Deep Q-Learning,” 2021, arXiv preprint arXiv:2103.15084. [Online]. Available: <https://arxiv.org/abs/2103.15084>
- [28] M. A. Nielsen and I. L. Chuang, *Quantum Computation and Quantum Information: 10th Anniversary Edition*. Cambridge Univ Press, 2010.
- [28] G. Brockman *et al.*, “OpenAI Gym,” 2016, arXiv preprint arXiv:1606.01540. [Online]. Available: <http://arxiv.org/abs/1606.01540>
- [29] H. van Hasselt, A. Guez, and D. Silver, “Deep Reinforcement Learning with Double Q-Learning,” in *AAAI Conf. on Artificial Intelligence*, vol. 30, no. 1, 2016.
- [30] M. Schuld and F. Petruccione, *Supervised Learning with Quantum Computers*. Springer International Publishing, 2018.
- [31] I. Cong, S. Choi, and M. D. Lukin, “Quantum Convolutional Neural Networks,” *Nature Physics*, vol. 15, no. 12, pp. 1273–1278, 2019.
- [32] Y. Liu, S. Arunachalam, and K. Temme, “A rigorous and robust quantum speed-up in supervised machine learning,” *Nature Physics*, vol. 17, no. 9, pp. 1013–1017, 2021.
- [33] V. Mnih *et al.*, “Human-Level Control through Deep Reinforcement Learning,” *Nature*, vol. 518, no. 7540, pp. 529–533, 2015.
- [34] C. J. C. H. Watkins, “Learning From Delayed Rewards,” Ph.D. dissertation, King’s College, Cambridge United Kingdom, 1989.
- [35] L.-J. Lin, “Self-Improving Reactive Agents Based On Reinforcement Learning, Planning and Teaching,” *Machine learning*, vol. 8, no. 3–4, pp. 293–321, 1992.
- [36] M. Cerezo *et al.*, “Variational quantum algorithms,” *Nature Reviews Physics*, vol. 3, no. 9, p. 625–644, Aug 2021.
- [37] J. R. McClean, J. Romero, R. Babbush, and A. Aspuru-Guzik, “The Theory of Variational Hybrid Quantum-Classical Algorithms,” *New J. Phys.*, vol. 18, no. 2, p. 023023, 2016.
- [38] A. Peruzzo *et al.*, “A Variational Eigenvalue Solver on a Photonic Quantum Processor,” *Nat Commun*, vol. 5, no. 1, p. 4213, 2014.
- [39] K. Mitarai, M. Negoro, M. Kitagawa, and K. Fujii, “Quantum Circuit Learning,” *Physical Review A*, vol. 98, no. 3, 2018.
- [40] M. Schuld, R. Sweke, and J. J. Meyer, “Effect of Data Encoding on the Expressive Power of Variational Quantum-Machine-Learning Models,” *Physical Review A*, vol. 103, no. 3, p. 032430, Mar. 2021.
- [41] M. Cerezo, A. Sone, T. Volkoff, L. Cincio, and P. J. Coles, “Cost Function Dependent Barren Plateaus in Shallow Parametrized Quantum Circuits,” *Nature Communications*, vol. 12, no. 1, 2021.
- [42] I. R. Khan and R. Ohba, “Closed-Form Expressions for the Finite Difference Approximations of First and Higher Derivatives Based on Taylor Series,” *Journal of Computational and Applied Mathematics*, vol. 107, no. 2, pp. 179–193, 1999.
- [43] M. Schuld, V. Bergholm, C. Gogolin, J. Izaac, and N. Killoran, “Evaluating analytic gradients on quantum hardware,” *Phys. Rev. A*, vol. 99, no. 3, 2019.
- [44] X.-Z. Luo, J.-G. Liu, P. Zhang, and L. Wang, “Yao.jl: Extensible, Efficient Framework for Quantum Algorithm Design,” *Quantum*, vol. 4, p. 341, Oct. 2020.
- [45] A. Pérez-Salinas, A. Cervera-Lierta, E. Gil-Fuster, and J. I. Latorre, “Data Re-Uploading for a Universal Quantum Classifier,” *Quantum*, vol. 4, p. 226, 2020.
- [46] E. Coumans and Y. Bai, *PyBullet, a Python Module for Physics Simulation for Games, Robotics and Machine Learning*, 2016. [Online]. Available: <http://pybullet.org>
- [47] J. R. McClean, S. Boixo, V. N. Smelyanskiy, R. Babbush, and H. Neven, “Barren plateaus in quantum neural network training landscapes,” *Nature Communications*, vol. 9, no. 1, 2018.
- [48] R. LaRose and B. Coyle, “Robust data encodings for quantum classifiers,” *Physical Review A*, vol. 102, no. 3, 2020.